# Composite Hydrogels Laden with Crystalline Active Pharmaceutical Ingredients of Controlled Size and Loading

Huseyin Burak Eral, Marcus O'Mahony, Robert Shaw, Bernhardt L. Trout, Allan S. Myerson, and Patrick S. Doyle*

Department of Chemical Engineering, Massachusetts Institute of Technology, 77 Massachusetts Avenue, Room 66-270, Cambridge, Massachusetts 02139, United States

S *Supporting Information*

ABSTRACT: Efficient control of crystallization and crystal properties still represents a bottleneck in the manufacturing of crystalline materials ranging from pigments to semiconductor particles. In the case of pharmaceutical drug manufacture, current methods for controlling critical crystal properties such as size and morphology that dictates the product's efficacy are inefficient and often lead to the generation of undesirable solid

states such as metastable polymorphs or amorphous forms. In this work, we propose an approach for producing crystals of a poorly water-soluble pharmaceutical compound embedded in a polymer matrix. Taking advantage of the composite hydrogel structure, we control the crystallization of the active pharmaceutical ingredient (API), within the composite hydrogel, generating crystalline API of controlled crystal size and loading. The composite hydrogels initially consist of organic phase droplets, acting as crystallization reactors, embedded in an elastic hydrogel matrix. By controlled evaporation of this composite material, crystals of controlled size (330 nm to 420 μm) and loading (up to 85%w/w) are produced. Through the interplay of elasticity and confinement, composite hydrogels control the crystal size and morphology via a two-step mechanism. First, the elastic matrix counteracts evaporation-induced coalescence of the emulsion droplets, keeping droplets isolated. Second, a confinement-induced elastic energy barrier, limits the growth of crystals beyond the size designated by the droplets. The proposed approach can be applied to production of a wide range of crystalline materials.
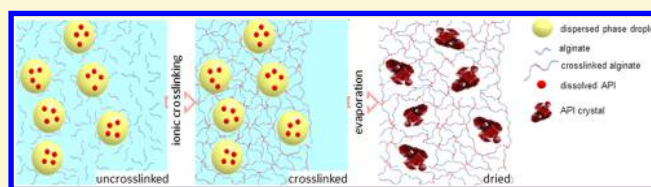
INTRODUCTION

Innovative use of materials has played a crucial role in the development of new fields ranging from advanced drug delivery[1,2] to biomimetic nanotechnology.[3−5] Novel materials such as microgels and mesoporous silica provide fine control over in vivo drug release rate.[6] These systems can carry a cargo to a predefined location in the body[7,8] and even evade detection from the immune system.[9,10] However, in the manufacturing of crystalline materials, especially pharmaceuticals, use of innovative material technology has not yet been extensively explored as in other fields. Controlling crystallization, particularly controlling crystal size and morphology, is critical in the manufacture of crystalline materials. The optical properties of nanoparticles,[11−14] the efficiency of explosives,[15] and pigments and catalyst[16] are intimately related their crystal size.

Recently, continuous manufacturing trends have pushed the boundaries in pharmaceutical manufacturing, promising lower costs, and improved sustainability.[17] These trends have initiated development of manufacturing processes utilizing advanced materials that can potentially provide previously unattainable control over critical pharmaceutical properties, such as solid form purity, final dosage formulation, and processability. Advanced materials can also help in transforming current manufacturing schemes into continuous more efficient processes while satisfying stringent industrial requirements.

Controlling the level of supersaturation in the crystallization of a melt, vapor, or solution phase is typically utilized to control the size of the resultant crystals. Techniques such as spray drying, supercritical fluid crystallization, and impinging jet crystallization create very high supersaturation levels to generate small crystals where nucleation is favored over crystal growth.[18] It is well-recognized that high supersaturation can lead to the formation of an undesired metastable crystalline phase(s) or amorphous noncrystalline material rather than an often preferred thermodynamically stable phase. Another approach to attaining crystals of desired size, comminution, can be used to decrease crystal size, postcrystallization. This involves use of high-energy processes such as milling and high pressure homogenization (in the presence of surfactants).[19−21] These cost ineffective and time-consuming techniques can subject crystals to large amounts of kinetic energy that can again induce the formation of undesirable amorphous or metastable crystal phases,[22] which can compromise stability and the bioavailability of pharmaceuticals.[22−24] Self-assembled monolayers[23] and porous glass[25] have been proposed for controlling crystal size and polymorphic form of a compound.
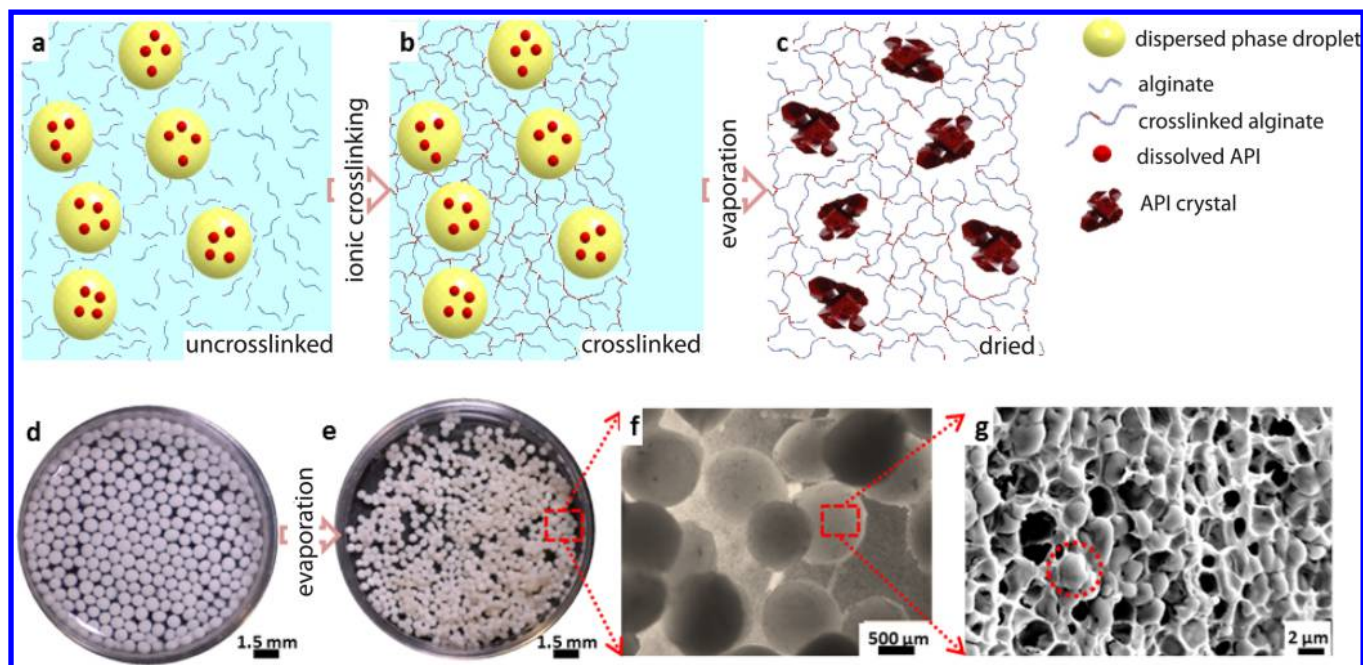
Figure 1. Illustration of bottom-up approach: The emulsion droplets carrying hydrophobic API are dispersed in aqueous solvent containing un-cross-linked polymer alginate. (b) Upon cross-linking, the (nano- or macro-) emulsion droplets are entrapped in the elastic hydrogel matrix. (c) Upon evaporation, dissolved API in emulsion droplets crystallizes to form crystals that are embedded in the dried hydrogel matrix. Panels d and e show hydrated "cross-linked" and "dried" composite hydrogels, respectively. (f) Microscopy images of "dried" composite hydrogels and (g) SEM image of "dried" composite hydrogel sliced open with embedded API identified (red circle).

However, soft materials such as polymer hydrogels remain largely unexplored in this respect.

Polymer hydrogels have been widely exploited in controlled drug release[6,26] and more recently as heteronucleants to control crystallization from solution.[27−29] However, due to their intrinsically hydrated (hydrophilic) nature, development of hydrogel materials capable of storing or interacting with hydrophobic (water insoluble) APIs[30] remains a challenge.[31] Forty-three percent of all pharmaceutical moieties, including cancer pharmaceuticals produced since 1980, are considered hydrophobic. Therefore, it is essential to develop novel manufacturing approaches for hydrophobic drugs[32] while addressing practical industrial challenges such as ensuring crystallinity of APIs, scale of production, high API loading, and flexibility to adjust the formulated dose.

This study describes a novel approach (Figure 1) for producing crystals of a poorly water-soluble pharmaceutical with controlled crystal size and loading embedded in a polymer matrix utilizing the unique structure of a novel biocompatible soft material: composite hydrogels. These materials consist of hydrophobic (organic phase) droplets acting as crystallization reactors embedded in a hydrogel matrix where the poorly water-soluble pharmaceutical can be dissolved at high concentrations. By controlled evaporation of this composite material, crystals of controlled size (330 nm to 420 μm) are produced. Adjustable loading of API crystals (up to 85% by weight) is achieved through careful selection of the organic phase, surfactant and cross-linking polymer alginate (ALG). We show that crystal size is dictated by the droplet size of nano- and macroemulsions trapped within the hydrogel matrix and by the concentration of the API dissolved in emulsion droplets. Control of crystal size and morphology is achieved via a two-step mechanism. First, the elastic nature of the hydrogel matrix counteracts evaporation-induced coalescence of emulsion

droplets, keeping droplets isolated. Second, a confinement-induced elastic energy barrier, dictating the crystal size and morphology, limits the growth of crystals beyond the size designated by the droplets. In a broader sense, a novel material-based approach is proposed to control crystal size and morphology in evaporation-induced crystallization —a widely used technique in material science and engineering.

■ EXPERIMENTAL SECTION

Materials. Anisole (CAS# 100−66−3, purity >99%), ethyl acetate (CAS# 141−78−6, purity >99%), fenofibrate (FEN, CAS# 49562−28−9, purity >99%), heptane (CAS# 142−82−5), and calcium chloride (CAS# 10043−52−4) were all purchased from Sigma-Aldrich and used as is. Surfactants pluronic surfactant (F68,CAS# 9003−11−6), sodium dodecylsulfate (SDS, CAS# 151−21−3) were purchased from Sigma-Aldrich used with no further treatment. Sodium Alginate (CAS# 9005−38−3) a polysaccharide consisting of approximately 61% mannuronic (M) and 39% guluronic (G) acid was purchased from Sigma. Thirty gauge needles were purchased from Nordson EFD. The parts for constructing the millifluidic setup, i.e., T-junction, quick connects are purchased from Upchurch scientific.

Procedure for composite hydrogels: The composite hydrogels were prepared by first dissolving the model API in the organic dispersed phase anisole containing the desired amount of dissolved FEN. The amount of FEN dissolved in anisole was adjusted by directly using or diluting a mother batch of anisole saturated with FEN. The mother batch of anisole saturated with FEN, i.e., $C_{FEN} = C_{satFEN}$, was prepared by bringing excessive amounts of FEN in contact with anisole hence establishing solid−liquid equilibrium at room temperature. The solubility of FEN in ANI was measured by evaporating a known volume of FEN saturated ANI at 60 °C in a vacuum oven. The mother batch was allowed to equilibrate for 24 h at room temperature at 200 rpm stirring speed. The organic dispersed phase was then emulsified in an aqueous continuous phase containing 2% weight by volume alginate (ALG), 5% weight by volume pluronic surfactant F68. The un-cross-linked mixture was then dripped into a water bath (10 cm diameter 2 cm deep) using 30G needles containing 6% by weight CaCl₂. For
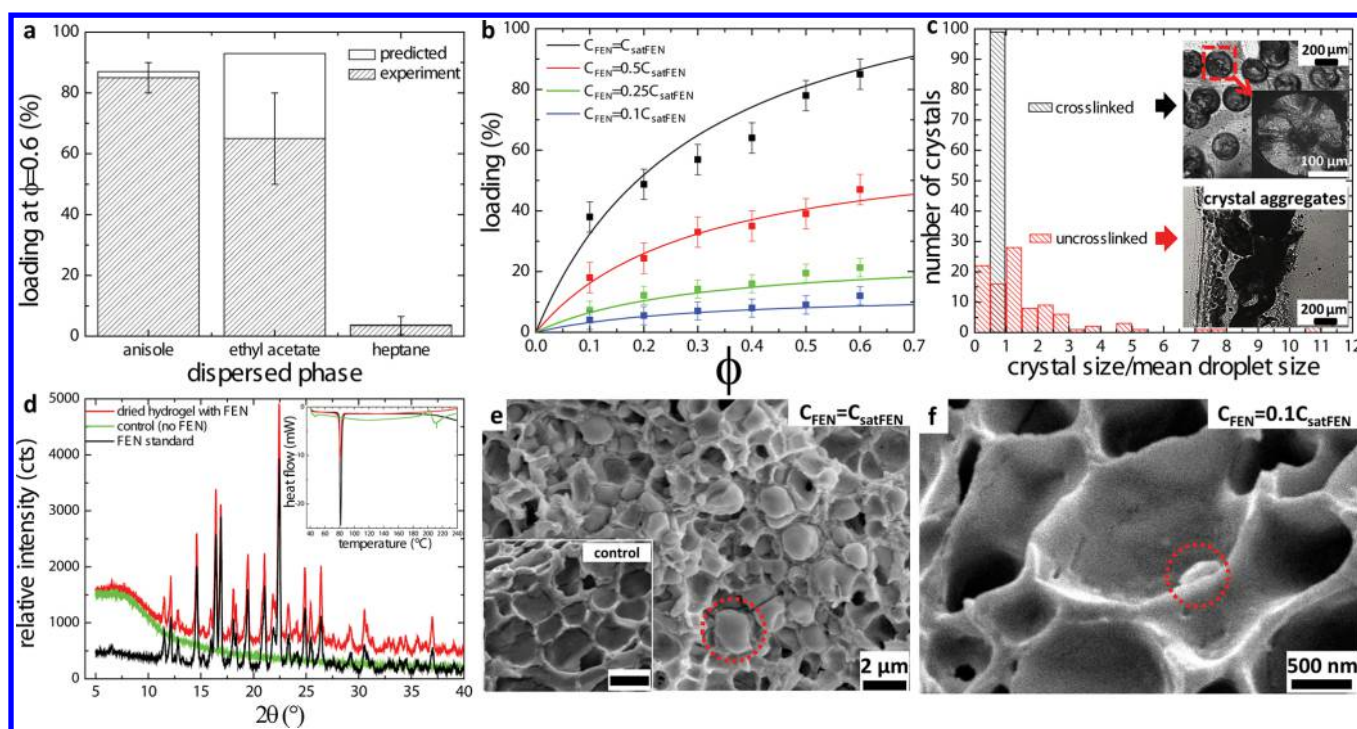
Figure 2. (a) Choosing the optimal dispersed phase anisole: Loading % of FEN (mass of API per mass of the dried composite hydrogel) with different dispersed phases is shown at ϕ = 60%. (b) Tunable loading: Loading % versus volume fraction (ϕ) on dry basis is plotted for different concentrations of API dissolved in anisole. (c) Hydrogel matrix counteracts evaporation-induced aggregation: The size distribution of crystals forming upon evaporation normalized by mean droplet size for un-cross-linked and cross-linked samples. The inset shows the microscopy images of the final residues and a cross-polarized microcopy image where crystalline regions appear bright (see the Supporting Information, S1 and Movies 1 and 2). (d) XRD and DSC (inset panel a) of dried typical composite hydrogel formulation (ϕ = 10% ANI dispersed in 2%w/v ALG and 5%w/vF68 $C_{FEN} = C_{satFEN}$), FEN standard and the control sample, i.e., dried typical composite hydrogel formulation without FEN. (e) SEM image of a typical formulated sample (sample crystal circled) and control without FEN with scale bar 2 μm (inset). (f) Submicrometer crystal (circled feature) prepared by diluting the concentration of FEN ($C_{FEN} = 0.1C_{satFEN}$) in the typical formulation.

dripping, the 3 mL syringes filled with uncrosslinked solution were dripped using a microfluidic positive displacement pump (KD Scientific 110). The dripping height was set to 10 cm and the dripping bath containing 6% CaCl$_2$ was stirred with a magnetic stirrer at 100 rpm. The resulting composite hydrogels were approximately 700 μm in size with 10% polydispersity.

The composite hydrogels were then washed by exchanging the calcium chloride cross-linking solution 5 times with deionized water. They were then filtered using a Buchner funnel and rinsed once more with deionized water. The composite hydrogels were gently pat-dried using blotting paper before removing to a vacuum oven at 60 °C for drying over 3−5 days.

Emulsification methods: To achieve different droplet sizes we used three different techniques namely (i) high pressure homogenization to make nanoemulsions, (ii) millifluidics to make monodispersed macroemulsion droplets, and (iii) magnetic stirring to make relatively large macroemulsions. To prepare the nanoemulsions, a crude macroemulsion was first generated as previously described[33,34] by adding the dispersed phase into the continuous phase. This crude macroemulsion was then homogenized using high pressure homogenization (Aventis emulsiFlex-C3) at two different applied pressures namely 5 and 15kPsia with 15 passes.

A millifluidics setup constructed as described before[24] (see the Supporting Information, S5), produced droplets sizes ranged between 100−500 μm. The uncrosslinked emulsion containing droplets produced by millifluidics were directly dripped into CaCl$_2$ solution to prepare composite hydrogel beads. Magnetic stirring was also used to make composite hydrogels. The dispersed phase was added into a 100 mL flask containing the continuous phase in a dropwise fashion using a buret. The droplets of the dispersed phase were then emulsified by a magnetic stirrer rotating at 400 rpm. The uncrosslinked solution is then loaded to syringes with 30G needles

and composite hydrogel beads are produced by dripping as described before.

Nanoemulsion characterization: Nanoemulsion droplet sizes were measured via dynamic light scattering using a Brookhaven Instruments BI-200SM multiangle apparatus. Samples were diluted to ϕ= 0.0005 in deionized water. Autocorrelation functions were measured at a scattering angle of 90° and a temperature of 25 °C.

Analysis of composite hydrogels material: The dried composite hydrogels were analyzed by powder X-ray diffraction (PXRD) in reflectance mode (Panalytical X'pert MPD Pro). The samples were ground placed on a zero background disk and analyzed from 4 to 40° 2θ using Cu α radiation. Samples were also analyzed by differential scanning calorimetry (DSC) using TA Instruments Q2000 DSC 2−5 mg of sample was weighed into a Tzero aluminum pan and sealed. These samples were then scanned 40−250 °C at 10 °C/min. For SEM images, we sliced open dried composite hydrogels beads using a razor and tweezers and we have taken over 10 images per bead along the diameter passing through the center. This process was repeated over five beads per formulation. The images were later analyzed with ImageJ manually to calculate the mean crystal size.

Dissolution Experiments: The in vitro dissolution of FEN from the prepared composite hydrogels was carried out using the standard USPII (paddle) apparatus at 37 °C, 75 rpm and pH 6.8. The pH value was chosen so that the hydrogels would be encouraged to swell[35,36] and with the uptake of water consequently release their drug contents. 600 mL dissolution media was prepared from sodium phosphate monobasic and dibasic stock solutions (0.2M) mixed in the appropriate ratios to obtain the desired pH and 0.72% w/v SDS was added as surfactant for the dissolution of hydrophobic FEN in the aqueous media.[37] Twenty-five milligrams ($\pm$0.5 mg) of dried typical composite hydrogel formulation was added to the dissolution media manually. Given the loading of FEN and the saturation concentration

of FEN in the media,[37] the mass of FEN added for a dissolution experiment was at least 3 times less than the mass of FEN required to saturate the media thus ensuring sink conditions during dissolution. The UV measurements were done automatically using an automatic Varian UV−vis Cary 50 apparatus and in situ probe set. All reported measurements were repeated 5 times under identical conditions and averaged values are given in Figure 3.

Loading measurements: The emulsion laden hydrogels are synthesized with different emulsion volume fractions ranging between 10 and 50% as described before. The volume fraction (ϕ) is defined as the volume of the dispersed phase, i.e., anisole, relative to the continuous phase, i.e., aqueous ALG solution. For each measurement of a given volume fraction, two batches of emulsion laden hydrogels are prepared with the same method of emulsification followed by cross-linking: reference batch without API, i.e., $C_{FEN} = 0$ and test batch carrying dissolved API at desired concentration. Both batches containing approximately 200 mg of ALG beads are pat-dried and weighted. The samples containing both batches are placed in vacuum oven and dried over 2 days at 60 °C. Loading is defined as the difference in weight between the dried test batch carrying API and the dried reference batch formulated without the API divided by the weight of the dried test batch carrying API. Loading is a function of the FEN concentrations (C_{FEN}) and the volume fraction (ϕ). The mass of FEN (m_{FEN}) in a hydrogel bead with volume V is given by $C_{FEN}V\phi$. The loading % is defined as the mass of FEN divided by the mass of dried hydrogel. To estimate the variation in loading and significance of variation, we repeated loading measurements in ten replicates (see the Supporting Information, S3).

RESULTS AND DISCUSSIONS

The following approach was developed to produce crystals of controlled size and loading of a model hydrophobic API (Fenofibrate, FEN): FEN is dissolved in an organic solvent (Anisole, ANI) that has been approved for pharmaceutical manufacture. FEN is chosen as a model hydrophobic drug due to its extremely low water solubility (0.3 μg/mL at 37 °C).[38] Nano- and macroemulsions are prepared by emulsifying the FEN-carrying hydrophobic organic phase in aqueous solution containing biocompatible polymer alginate (ALG) and biocompatible surfactant pluronic F68 (Figure 1a "un-cross-linked"). ALG beads (mean diameter 700 μm ± 70) are produced by dripping the uncrosslinked sample into 6% w/v (weight/volume) CaCl$_2$ bath in dropwise fashion.[39] Ionic cross-linking of ALG creates a crosslinked polymer network trapping the emulsion droplets (Figure 1b "crosslinked"). Crystallization of FEN is induced by controlled evaporation of both the dispersed organic phase and the aqueous phase (Figure 1c "dehydrated") at 60 °C. The evaporation temperature was below the melting temperature of the target compound for effective evaporation-induced crystallization (see the Supporting Information, S3). Once the aqueous and dispersed phases evaporate, crystals filling the dried hydrogel matrix can be observed in Figure 1g when a dried bead (Figure 1e, f) is sliced open and imaged under SEM.

The highest loading of the model API is achieved where the following conditions (see the Supporting Information, S2) are met simultaneously: (i) the solubility of API in the dispersed phase should be high and (ii) the solubility of the dispersed phase in the continuous phase should be low or negligible. On the basis of the solubility of API in the dispersed phase, ethyl acetate appears to be a better option than anisole and heptane, indicated by predicted loading in Figure 2a. If ethyl acetate is chosen as the dispersed phase, ethyl acetate dissolves in water facilitating the precipitation of API in the continuous phase due to the high solubility of ethyl acetate in the continuous phase.

Hence ANI was chosen as the dispersed phase satisfying both conditions throughout this study. Composite hydrogels provide flexibility in adjusting the amount of API embedded, i.e., dosage in final formulation. The amount of FEN embedded in composite hydrogels (% loading on dry basis) can be controlled by tuning the volume fraction of the dispersed phase (ϕ, volume of dispersed phase within the total volume of the aqueous and the dispersed phases) and the concentration of hydrophobic API FEN (C_{FEN}) dissolved in the dispersed phase (see Figure 2b and the Supporting Information, S10). The C_{FEN} is given relative to saturation limit of FEN at room temperature ($C_{satFEN} \approx 400$ mg/mL). C_{FEN} is adjusted by diluting a saturated solution of FEN dissolved in the organic phase in equilibrium with solid FEN at room temperature. Adjustable and high loadings up to 85% can be achieved with relatively narrow distributions (<4%). In the manufacturing process of an API, flexibility to adjust the loading would enable easy adjustment of the dosage of a final formulation. The dried biocompatible composite hydrogels can be directly compressed to produce a tablet form (see the Supporting Information, S3 and Figure S2). Our composite hydrogels are amenable to continuous manufacturing. A lab-scale manufacturing scheme demonstrating the transferability of the proposed approach to industrial manufacturing is presented in the Supporting Information, S3. The maximum loading achieved with our composite hydrogels is, to the best of our knowledge, the highest loading capacity ever demonstrated in a hydrogel material with a hydrophobic API in crystalline form.

The hydrogel matrix counteracts the coalescence of emulsion droplets during the evaporation process ensuring uniform crystal size distribution. The behavior of composite hydrogels during evaporation was investigated uncrosslinked and cross-linked samples of a typical formulation (10% volume fraction ANI/FEN where $C_{FEN} = C_{satFEN}$ with 2%w/v ALG and 5%w/v pluronic surfactant F68) were sandwiched between two glass slides. These experimental samples were overnight under microscope at 60 °C (see the Supporting Information, S1 and Movies 1 and 2). Uniform size droplets of 210 μm diameter were produced by millifluidics[40] (Experimental Section). Insets in Figure 2c show the final residues left behind after 18 h. As the uncrosslinked sample evaporates, the droplets are carried to the center by the receding contact line due to evaporation (see the Supporting Information, S1 and Movie 1). They are brought into close contact and consecutively coalesce as the continuous phase evaporates. As seen in the inset of Figure 2c, the coalescence of API-carrying droplets results in crystal aggregates larger than the initial droplet size. These crystal aggregates produce nonuniform crystal size distributions (Figure 2c). In the crosslinked sample, the emulsion droplets cannot be carried or destabilized by evaporation as the hydrogel matrix counteracts the evaporation driven motion of the contact line, keeping the droplets fixed in place (see the Supporting Information, S1 and Movie 2). As the droplets do not coalesce, the crystal-size distribution within the dried hydrogel matrix is homogeneous (Figure 2c and inset). Narrow crystal-size distributions are preferable in industrial practice as they lead to well-characterized dissolution rates and product performance.

DSC and XRD were used to investigate the crystallinity of the API particles embedded in the dried composite hydrogels (Figure 2d). Both techniques demonstrate that the FEN contained within the dried hydrogel matrix is crystalline. In Figure 2d, XRD peaks of FEN standard matches the peaks of
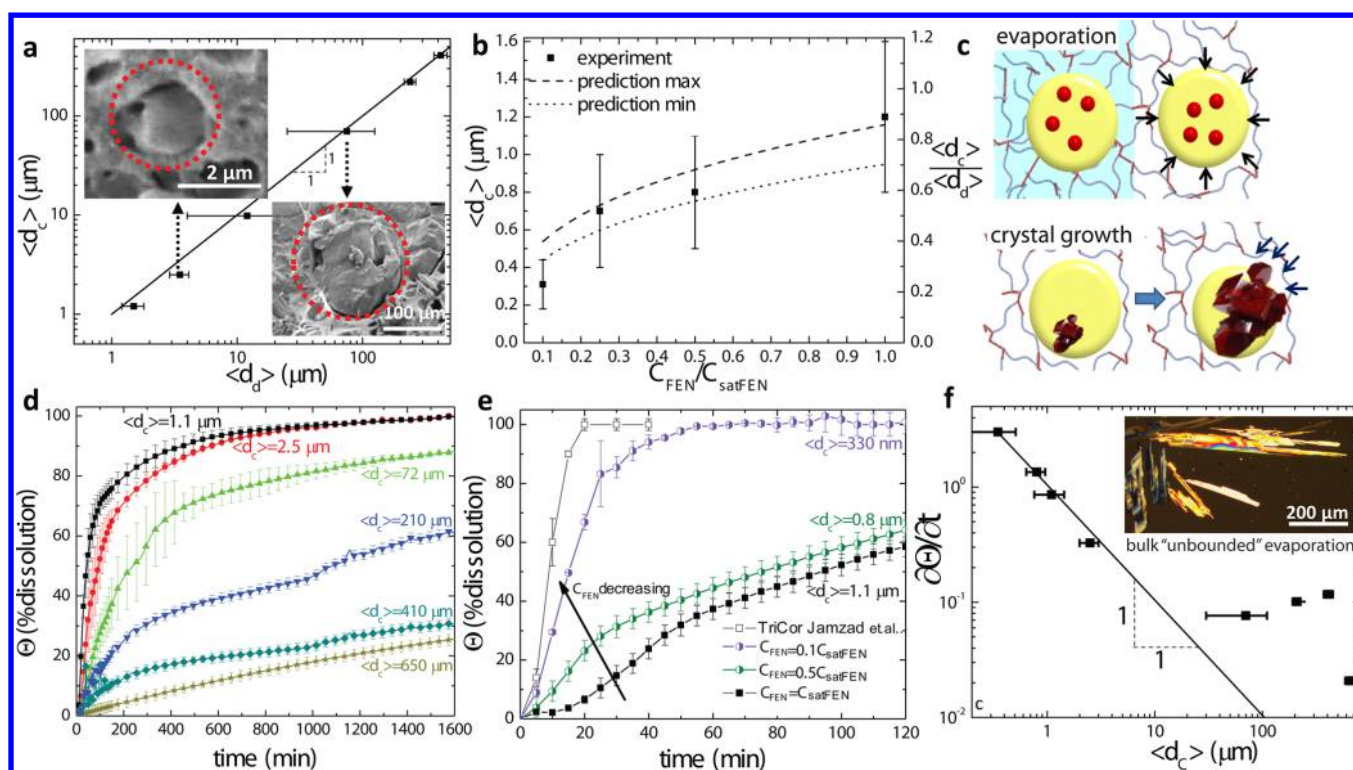
Figure 3. (a) Controlling the crystal size by controlling the droplet size at fixed API concentration ($C_{sat} = C_{satFEN}$): The mean crystal size ($\langle d_c \rangle$) plotted as a function of the mean droplet size ($\langle d_d \rangle$) insets show a SEM image of dried composite hydrogel containing nanoemulsions ($\langle d_c \rangle = 2.5$ μm) and macroemulsions ($\langle d_c \rangle = 72$ μm). (b) Controlling the crystal size through concentration of API within emulsions while keeping droplet size constant: The crystal size as a function of relative dilution ($C_{FEN} \backslash C_{satFEN}$). (c) Mechanistic explanation on the two-step effect of hydrogel matrix during evaporation of the aqueous phase and crystal growth. (d) Dissolution profile of dried composite hydrogels with different crystal sizes prepared by controlling the droplet size at fixed API concentration ($C_{sat} = C_{satFEN}$). The mean crystal sizes and polydispersities are 1.1 ± 0.2, 2.5 ± 0.5, 72 ± 45, 210 ± 12, 410 ± 21, and 650 ± 200 μm. (e) Dissolution profile of crystals prepared by controlling C_{FEN}/C_{satFEN} ratio for nanoemulsions of fixed droplet size $\langle d_d \rangle = 1.1$ μm. The mean diameter and polydispersity of each curve is 0.33 ± 0.17, 0.8 ± 0.2, and 1.1 ± 0.2 μm. (e) Rate of dissolution $d\Theta/dt$ ($t = 5$ min) as a function of mean crystal size for dissolution profiles shown in panels d and e. The inset shows needlelike crystals of FEN obtained by evaporating millimeter-sized ANI droplets, i.e., bulk "unbounded" evaporation-induced crystallization.

the typical formulation of dried composite hydrogel (ϕ =10% ANI/FEN with $C_{FEN} = C_{satFEN}$ emulsified in 2%w/v ALG and 5%w/v pluronic surfactant F68). The control sample containing no FEN, prepared under the same conditions as dried hydrogel with FEN shows no peaks indicating no crystalline structure is present. DSC measurement (inset of Figure 2d) further demonstrates the crystallinity of the FEN particles within the dried hydrogel matrix. Both the sample and the FEN standard show a single well-defined melting point at the same temperature, indicating the both samples are crystalline. The control sample prepared without FEN showed no well-defined melting point, only endo- and exothermic events associated with degradation of alginate and surfactant pluronic F68.[41]

The dried composite hydrogels were carefully sliced open and imaged with SEM revealing the fine structures within. Figure 2e shows that within the dried composite structure the spaces previously occupied by nanoemulsion droplets are filled with crystals of FEN. Figure 2e also shows some vacant cavities likely due to crystals having fallen out during SEM sample preparation. The control sample, prepared without FEN (inset of Figure 2e), shows only micrometer-sized vacant holes with no crystals inside. Dilution of the API concentration in the dispersed phase resulted in crystals that are smaller than the cavities left behind once the emulsion droplets have evaporated. Figure 2f shows a submicron crystalline FEN particle resulting

from a 1:10 dilution of the FEN saturated anisole solution, i.e., $C_{FEN} = 0.1 C_{satFEN}$ (see the Supporting Information, S6, for more SEM images and S9 for XRD data).

Controlling crystal size is of utmost importance as it controls pharmaceutical product performance characteristics such as in vivo dissolution rate and bioavailability. We hypothesized that the crystal size could be manipulated by controlling (i) the dispersed phase droplet size embedded within composite hydrogels and (ii) the concentration of API in the dispersed phase. To engineer the size of crystals embedded within composite hydrogels, we first systematically varied the droplet size keeping the FEN concentration constant ($C_{FEN} = C_{satFEN}$) and, using different emulsification techniques—high-pressure homogenization, millifluidics, and magnetic stirring—we created droplet diameters ranging from 1.1 to 410 μm. Upon evaporation of our composite material the mean size of FEN crystals formed was measure. In Figure 3a, we plot mean crystal size ($\langle d_c \rangle$) measured by SEM (and by optical microscopy where the crystals were large enough) as a function of mean droplet size ($\langle d_d \rangle$) measured by dynamic light scattering and microscopy. Figure 3a follows a straight line with slope one passing through the origin within error bars. This indicates that the size of embedded droplets within the hydrogel matrix dictates the mean crystal size within the dried hydrogel matrix. This is observed to be the case when the concentration of FEN in the dispersed phase (ANI) is the saturation concentration of

FEN in ANI ($C_{FEN} = C_{satFEN}$). Hence we deduced that as the liquid phases (both aqueous and dispersed organic phase) were evaporated, FEN crystals nucleated and began to grow within the dispersed phase droplets. The growth of these crystals is limited by the confinement of the hydrogel matrix and the size of the cavity left behind by the evaporating droplets. Consequently, the average size of droplets dictates the average size of embedded crystals at $C_{FEN} = C_{satFEN}$ in accordance with previous observations (Figure 2c). It is important to note that water evaporates faster that ANI, leaving ANI droplets embedded in a dehydrated matrix that is stiffer than the hydrated matrix. This stiffer matrix ensures that the droplets, and consequently the crystals, are confined. The XRD data of all formulations shown in Figure 3 can be found in the Supporting Information, S9.

The crystal size can also be engineered by controlling the concentration of FEN in droplets embedded in the composite hydrogel. The droplet size was kept constant ($\langle d_d \rangle = 1.1 \mu m$) and nanoemulsion laden composite hydrogels with different FEN concentration (C_{FEN}) in the dispersed phase (ANI) were prepared. The C_{FEN} is adjusted by diluting the ANI solution that has previously achieved equilibrium with FEN solid at room temperature. Upon SEM imaging of diluted samples, we observed smaller crystals than the typical formulation (Figure 2f). The mean crystal size is plotted as a function of normalized FEN concentration (C_{FEN}/C_{satFEN}) in Figure 3b. To validate our results, we estimated the expected crystal size based on the density of FEN crystals, nanoemulsion droplet size, the concentration and the size of droplets given in Figure 3b. The measured crystal sizes coincide with the expected crystal sizes within error bars. The maximum and minimum predictions account for the nanoemulsion droplet size polydispersity. The composite hydrogels achieve the crystal size and the morphology control by introducing an elastic energy barrier to counteract (i) evaporation induced droplet coalescence, and (ii) crystal growth (Figure 3c). First, the hydrogel matrix counteracts the coalescence of droplets as the aqueous phase evaporates by keeping the droplets isolated. In the absence of the hydrogel matrix, the droplets coalesce and form nonuniform crystal size distributions as shown in Figure 2c and Movies 1 and 2 in the Supporting Information. Second, the hydrogel matrix regulates the crystal growth by introducing a confinement-induced elastic energy barrier limiting the growth. In other words, the crystal cannot grow beyond the size of the emulsion without overcoming an elasticity induced energy barrier.

By controlling the crystal size embedded in the composite material, we demonstrate that we can control the release profile of FEN from composite hydrogels in Figure 3d. The in vitro dissolution profiles measured at 37 °C demonstrate the influence of crystal size on release rate. The larger crystals prepared by millifluidics and magnetic stirring result in slower release of API into the dissolution medium, whereas composite dried hydrogels formulated using nanoemulsions through high-pressure homogenization—producing smaller crystals—result in faster dissolution. With diluted samples (Figure 3b), the fastest dissolution rates were achieved (Figure 3e). The dissolution rate of the composite material containing crystals having an average size of 330 nm is comparable to the dissolution rate of the-state-of-the-art FEN formulation -commercialized as TriCor tablets (Figure 3e). These tablets are prepared by a nanomilling technique that generates submicron crystals[37] estimated to be approximately 400 nm

in size. It is important to note that tuning the crystal size through dilution decreases the loading—the maximum achieved loading at $C_{FEN} = 0.1 C_{satFEN}$ at $\phi = 60\%$ is 16% (Figure 2b). The polydispersity of the crystal size also influences the dissolution behavior in Figure 3d. (see the Supporting Information, S8, for a more detailed discussion).

For each dissolution profile presented in Figure 3, we fitted a semiempirical model commonly used in drug dissolution through polymer matrix[6] $\Theta = At^n$ − where Θ denotes percentage of drug dissolved, t is time, and A and n are fitting parameters (see the Supporting Information, S8). Then we calculated the rate of dissolution $d\Theta/dt$ at $t = 5$ min using this model. Plotting rate of dissolution with respect to mean crystal size $\langle d_c \rangle$ showed an increasing rate of dissolution with decreasing crystal size (Figure 3f). If the dissolution kinetics were dictated by the crystal size, we would expect the rate of dissolution to depend on the total surface area as suggested by the Noyes−Whitney equation.[42] Our dissolution experiments were performed with the same amount of hydrophobic API for different crystal sizes hence $d\Theta/dt$ vs $\langle d_c \rangle$ should scale with $1/\langle d_c \rangle$ (see the Supporting Information, S8). In Figure 3f, very good agreement is observed for all crystal sizes (i.e., engineered by controlling both the droplet size and the dilution (C_{FEN}/C_{satFEN}) except for larger crystal sizes. For larger crystals, higher than predicted dissolution rates are observed. This deviation might be attributed to larger crystals having different dominating crystal facets than the more confined smaller crystals. A crystal in a large droplet can grow over a larger distance (same order of magnitude as droplet diameter) hence the area of the fast growing facet to slow growing facet would be larger. Different crystal facets could give rise to different surface energies[43,44] and this may be responsible for the deviations seen for larger crystals in the dissolution profiles. It is recognized that modifications in crystal habit can affect in vitro dissolution profiles and pharmaceutical performance.[45] This deviation points to an interesting fundamental insight. Confinement not only influences crystal size but also crystal morphology. It is observed that if crystals of the API are allowed to grow unbounded (i.e., in bulk), they form needles (inset of Figure 3f) whereas the crystals confined to grow no larger than the emulsion droplets are forced to acquire other morphologies with different surface energies.

Manufacturing crystalline materials using composite hydrogels is a unique approach enabling precise control over crystal size. This is impossible to achieve in traditional evaporation induced crystallization where once crystal nucleation occurs, there is no mechanism to limit/control the crystal growth. The approach enables crystal size and morphology control through a two-step mechanism utilizing the elastic nature of the hydrogel matrix and confinement. It is fundamentally different than other approaches that use emulsions or gels to influence crystallization. Traditionally crystal growth in gels has been used to prepare single crystals of proteins by taking advantage of diffusion-limited mass transport conditions[46] or as 3D structural networks for hydrophilic compounds in matrix-mediated crystallization/biomineralization studies.[47] This approach is mechanistically different as the growing hydrophobic crystalline phase is confined by the hydrogel matrix through the elastic energy barrier that the hydrogel matrix creates.

■ CONCLUSIONS

A material based approach is described to enable control over the crystal size and morphology of a hydrophobic compound

(an API) utilizing the unique structure of composite hydrogels. By controlling the size of embedded emulsions and the concentration of hydrophobic pharmaceutical in emulsions, we achieve fine control over crystal size (as small as 330 nm). The dissolution profile of the API material embedded in these composite materials can be controlled on the basis of crystal size. Rapid dissolution rates comparable to a commercial formulation with submicrometer crystals produced by harsh and energy intensive nanomilling technique[48,49] were achieved. Compared to the state of the art techniques, our method avoids excessive energy input and high saturation levels that can lead to amorphous forms or the appearance of metastable crystal phases. Furthermore, adjustable loadings as high as 85% are demostrated. Because of their biofriendly nature, adjustable submicrometer crystal size, and high loading capacity, the preposed alginate composite hydrogels could potentially serve as a final drug formulation and their production is amenable to continuous manufacturing (see the Supporting Information, S3). We are currently exploring other ways of utilizing this biocompatible hydrogel material to affect crystal growth morphology, prepare crystalline material on the nanoscale, and further engineer API dissolution profiles for applications such as controlled release.

The proposed approach achieves control over crystal size and morphology in a distinct two-step mechanism utilizing elasticity and confinement provided by the structure of composite hydrogel. First, the elastic matrix counteracts evaporation-induced coalescence of the emulsion droplets, keeping droplets isolated. Second, a confinement-induced elastic energy barrier, limits the growth of crystals beyond the size designated by the droplets. The versatility and orthoganol accessability of the composite hydrogels opens up a wide range of applications such as the design of multidrug therapies and the preparation of designer foods. The proposed approach is not limited to pharmaceuticals, and it can be applied to production of a wide range of crystalline materials.

ASSOCIATED CONTENT

Ⓢ Supporting Information

Movies 1 and 2, experimental details and explanation of movies 1 and 2, detailed discussion about how to choose components, Tablet production from composite hydrogels and continuous manufacturing, details on evaporation experiments in Figure 2 and demonstration of the ability of the hydrogel matrix to counteract creaming or sedimentation. Millifluidics setup, additional SEM images and size analysis from SEM images, TGA and DSC analysis, discussion about dissolution profiles and models used to fit data, additional XRD measurements for all formulations used in experiments, detailed experimental procedures, and stability of ANI nanoemulsions. This material is available free of charge via the Internet at http://pubs.acs.org.

AUTHOR INFORMATION

Corresponding Author

*E-mail: pdoyle@mit.edu.

REFERENCES

(1) Langer, R.; Tirrell, D. A. *Nature* **2004**, *428*, 487−492.
(2) Gardner, C. R.; Walsh, C. T.; Almarsson, O. *Nat. Rev. Drug Discovery* **2004**, *3*, 926−934.
(3) Aizenberg, J. *Mrs. Bull.* **2010**, *35*, 323−330.
(4) Aizenberg, J.; Black, A. J.; Whitesides, G. H. *J. Am. Chem. Soc.* **1999**, *121*, 4500−4509.
(5) Demirors, A. F.; Pillai, P. P.; Kowalczyk, B.; Grzybowski, B. A. *Nature* **2013**, *503*, 99−103.
(6) Peppas, N. A.; Bures, P.; Leobandung, W.; Ichikawa, H. *Eur. J. Pharm. Biopharm.* **2000**, *50*, 27−46.
(7) Mo, R.; Sun, Q.; Xue, J. W.; Li, N.; Li, W. Y.; Zhang, C.; Ping, Q. N. *Adv. Mater.* **2012**, *24*, 3659−3665.
(8) Turkoglu, M.; Takka, S.; Baran, H.; Sakr, A. *Pharm. Ind.* **1999**, *61*, 662−665.
(9) Scott, M. D.; Murad, K. L. *Curr. Pharm. Design* **1998**, *4*, 423−438.
(10) Balmert, S. C.; Little, S. R. *Adv. Mater.* **2012**, *24*, 3757−3778.
(11) Alivisatos, A. P. *J. Phys. Chem.-Us* **1996**, *100*, 13226−13239.
(12) Yang, C. S.; Awschalom, D. D.; Stucky, G. D. *Chem. Mater.* **2001**, *13*, 594−598.
(13) Teranishi, T.; Miyake, M. *Chem. Mater.* **1998**, *10*, 594−600.
(14) Chane-Ching, J. Y.; Martinet, G.; Panteix, P. J.; Brochard, C.; Barnabe, A.; Airiau, M. *Chem. Mater.* **2011**, *23*, 1070−1077.
(15) Armstrong, R. W.; Coffey, C. S.; Devost, V. F.; Elban, W. L. *J. Appl. Phys.* **1990**, *68*, 979−984.
(16) Di Renzo, F. *Catal. Today* **1998**, *41*, 37−40.
(17) Mascia, S.; Heider, P. L.; Zhang, H. T.; Lakerveld, R.; Benyahia, B.; Barton, P. I.; Braatz, R. D.; Cooney, C. L.; Evans, J. M. B.; Jamison, T. F.; Jensen, K. F.; Myerson, A. S.; Trout, B. L. *Angew. Chem., Int. Ed.* **2013**, *52*, 12359−12363.
(18) Mahajan, A. J.; Kirwan, D. J. *J. Phys. D. Appl. Phys.* **1993**, *26*, B176−B180.
(19) Chen, J.; Sarma, B.; Evans, J. M. B.; Myerson, A. S. *Cryst. Growth Des.* **2011**, *11*, 887−895.
(20) Peltonen, L.; Hirvonen, J. *J. Pharm. Pharmacol.* **2010**, *62*, 1569−1579.
(21) de Waard, H.; Hinrichs, W. L. J.; Frijlink, H. W. *J. Controlled Release* **2008**, *128*, 179−183.
(22) Lee, A. Y.; Erdemir, D.; Myerson, A. S. *Annu. Rev. Chem. Biomol.* **2011**, *2*, 259−280.
(23) Lee, A. Y.; Lee, I. S.; Dettet, S. S.; Boerner, J.; Myerson, A. S. *J. Am. Chem. Soc.* **2005**, *127*, 14982−14983.
(24) Leon, R. A. L.; Wan, W. Y.; Badruddoza, A. M.; Hatton, T. A.; Khan, S. A. *Cryst. Growth Des.* **2014**, *14*, 140−146.
(25) Ha, J. M.; Wolf, J. H.; Hillmyer, M. A.; Ward, M. D. *J. Am. Chem. Soc.* **2004**, *126*, 3382−3383.
(26) Aaltonen, J.; Alleso, M.; Mirza, S.; Koradia, V.; Gordon, K. C.; Rantanen, J. *Eur. J. Pharm. Biopharm.* **2009**, *71*, 23−37.
(27) Diao, Y.; Helgeson, M. E.; Myerson, A. S.; Hatton, T. A.; Doyle, P. S.; Trout, B. L. *J. Am. Chem. Soc.* **2011**, *133*, 3756−3759.
(28) Diao, Y.; Whaley, K. E.; Helgeson, M. E.; Woldeyes, M. A.; Doyle, P. S.; Myerson, A. S.; Hatton, T. A.; Trout, B. L. *J. Am. Chem. Soc.* **2012**, *134*, 673−684.
(29) Eral, H. B.; Lopez, V.; O'Mahoney, M.; Trout, B. L.; Myerson, A. S.; Doyle, P. S. *Cryst. Growth Des.* **2014**, *14*, 2073−2082.
(30) Lipinski, C. A.; Lombardo, F.; Dominy, B. W.; Feeney, P. J. *Adv. Drug Deliver Rev.* **2012**, *64*, 4−17.
(31) An, H. Z.; Helgeson, M. E.; Doyle, P. S. *Adv. Mater.* **2012**, *24*, 3838−3844.
(32) Josef, E.; Zilberman, M.; Bianco-Peled, H. *Acta. Biomater.* **2010**, *6*, 4642−4649.
(33) An, H. Z.; Safai, E. R.; Eral, H. B.; Doyle, P. S. *Lab. Chip* **2013**, *13*, 4765−4774.

6219

dx.doi.org/10.1021/cm502834h | *Chem. Mater.* 2014, 26, 6213−6220

(34) Helgeson, M. E.; Moran, S. E.; An, H. Z.; Doyle, P. S. *Nat. Mater.* **2012**, *11*, 344−352.

(35) Yotsuyanagi, T.; Ohkubo, T.; Ohhashi, T.; Ikeda, K. *Chem. Pharm. Bull.* **1987**, *35*, 1555−1563.

(36) Yotsuyanagi, T.; Yoshioka, I.; Segi, N.; Ikeda, K. *Chem. Pharm. Bull.* **1991**, *39*, 1072−1074.

(37) Jamzad, S.; Fassihi, R. *AAPS Pharmscitech* **2006**, *7*.

(38) Vogt, M.; Kunath, K.; Dressman, J. B. *Eur. J. Pharm. Biopharm.* **2008**, *68*, 283−288.

(39) Takka, S.; Acarturk, F. *J. Microencapsul.* **1999**, *16*, 275−290.

(40) Uspal, W. E.; Burak Eral, H.; Doyle, P. S. *Nat. Commun.* **2013**, *4*, 2666.

(41) Caykara, T.; Demirci, S.; Eroglu, M. S.; Guven, O. *Polymer* **2005**, *46*, 10750−10757.

(42) Noyes, A. A. W.; W, R. *J. Am. Chem. Soc.* **1897**, *19*, 930−934.

(43) Heng, J. Y. Y.; Bismarck, A.; Williams, D. R. *AAPS Pharmscitech.* **2006**, *7*.

(44) Heng, J. Y. Y.; Williams, D. R. *Langmuir* **2006**, *22*, 6905−6909.

(45) Modi, S. R.; Dantuluri, A. K. R.; Puri, V.; Pawar, Y. B.; Nandekar, P.; Sangamwar, A. T.; Perumalla, S. R.; Sun, C. C.; Bansal, A. K. *Cryst. Growth Des.* **2013**, *13*, 2824−2832.

(46) Garcia-Ruiz, J. M.; Gavira, J. A.; Otalora, F.; Guasch, A.; Coll, M. *Mater. Res. Bull.* **1998**, *33*, 1593−1598.

(47) Asenath-Smith, E.; Li, H. Y.; Keene, E. C.; Seh, Z. W.; Estroff, L. A. *Adv. Funct. Mater.* **2012**, *22*, 2891−2914.

(48) Gao, L.; Zhang, D. R.; Chen, M. H. *J. Nanopart. Res.* **2008**, *10*, 845−862.

(49) Moschwitzer, J.; Muller, R. H. *J. Nanosci. Nanotechnol.* **2006**, *6*, 3145−3153.

6220

dx.doi.org/10.1021/cm502834h | *Chem. Mater.* 2014, 26, 6213−6220